J. MACROMOL. SCI.—PHYS., B36(3), 345-355 (1997)

Light Scattering Study of Spherical Poly(*N*-isopropylacrylamide) Microgels

CHI WU* and SHUIQIN ZHOU
Department of Chemistry
The Chinese University of Hong Kong
Shatin, N. T., Hong Kong

ABSTRACT

Nearly monodisperse spherical microgel particles of poly(*N*-isopropylacrylamide) (PNIPAM) were prepared by emulsion polymerization in water. The volume phase transition of the microgel particles was studied by static and dynamic laser light scattering (LLS) in terms of the radius of gyration (R_g) and hydrodynamic radius (R_h). The phase transition temperature of the microgel ~33.0°C, similar to that of individual PNIPAM chains in water. The temperature independence of R_g/R_h(~0.78 ± 0.03) shows that in both the swollen and collapsed states the microgels are uniform particles behaving as hydrodynamically equivalent spheres. About 94% of the water inside the microgel network is driven out during the phase transition. The volume change of the microgel particles is continuous, in contrast to the discontinuous volume change observed in some bulk PNIPAM gels. The microgel particles are thermodynamically stable even at their collapsing limit. The behavior of microgel particles is compared to that of individual PNIPAM chains.

INTRODUCTION

Since Dusek and Patterson predicted the possibility of a discontinuous volume change of a polymer gel in analogy to the coil-to-globule transition [1] the volume phase transition of polymer gels has attracted much attention [2-5]. Remarkable progress has been made in the understanding of the phase transitions and critical phenomena in polymer gels. It has been reported that some polymer gels can swell

*To whom correspondence should be addressed.

or shrink discontinuously and reversibly in response to many different stimuli, such as temperature [6], pH [7], electric fields [8], or light [9], depending on the chemical composition of a given gel/solvent system. The volume change can be as large as a 1000-fold [10]. The large volume change of polymer gels in response to an infinitesimal alternation in environment may also be utilized in controlled release of biological molecules at specific body conditions, with selective absorbents, chemical memories, sensors, and artificial muscles.

Poly(*N*-isopropylacrylamide) (PNIPAM) gels have been extensively studied [13–26]. Their volume can change a 100-fold in water when the temperature varies only ~ 1–2° [11,12]. Several models have been proposed to explain the value phase transition. The earliest prediction of the collapse of the PNIPAM gel was made by Hirotsu et al. [13], and recently they have considered the concentration dependence of the Flory interaction parameter χ which can make the phase transition possible within the Flory–Huggins incompressible lattice model [14]. However, this model cannot explain the experimental data in the collapsed regime since it neglects the volume changes of mixing and the topological constraints of the gel network. Marchetti et al. [16] introduced the lattice vacancy and finite chain extensibility to allow for a nonzero volume change of mixing, so that the data from larger deformation of the gels can be reasonably fitted. Considering the gel collapse as the coil-to-globule transition of subchains, Grosberg et al. [17] discussed the contribution of topological constraints to this process. Their theory can satisfactorily describe part of the results in the phase transition range. The diversity of theories shows that a better understanding of the volume phase transition of the PNIPAM gels is required.

So far, most experimental studies have dealt with the swelling and shrinking of bulk PNIPAM gels by using various methods, such as microscopy [18], dilatometry [19], differential scanning calorimetry [20], friction measurement [21], small-angle neutron scattering [22], and nuclear magnetic resonance (NMR) [23]. Only a very few studies of PNIPAM microgels have been reported [24–27]. Tanaka et al. [20] showed that for a spherical gel, the time required for swelling of shrinking is proportional to the square of its radius. Microgel particles with a small radius will have a much faster response to a change of the environment. The phase transition of gels is a macroscopic manifestation of the coil-to-globule transition of individual linear chains. Therefore, a comparison between the PNIPAM gel networks and individual PNIPAM linear chains in water will improve our understanding of swelling and shrinking at the molecular level.

In this study, nearly monodisperse spherical PNIPAM microgel particles (R_h ~ 180 nm) were prepared by emulsion polymerization. Their volume phase transition was studied by both static and dynamic laser light scattering (LLS). A comparison of the properties of the microgel particles with those of individual PNIPAM chains in water is presented.

THEORETICAL BACKGROUND

Thermodynamics of the Volume Phase Transition of Gels

The swelling and collapse of a polymer gel can be characterized by the linear expansion factor $\alpha = (V/V_o)^{1/3} = (\phi_T/\phi_\Theta)^{1/3}$, where ϕ_Θ and ϕ_T are the volume fractions of the gel networks at the temperature Θ and T, respectively. In the mean

field theory the free energy (ΔF) of a neutral polymer network has two parts [4,16], that is:

$$\Delta F = \Delta F_m + \Delta F_{el} \tag{1}$$

with

$$\Delta F_m = k_B T[(1 - \phi)\ln(1 - \phi) + \chi\phi - \chi\phi^2] \tag{2}$$

and

$$\Delta F_{el} = \frac{3k_B T}{2N}\left[\left(\frac{\phi_0}{\phi}\right)^{2/3} - 1 - \ln\left(\frac{\phi_0}{\phi}\right)\right] \tag{3}$$

where ΔF_m and ΔF_{el} represent the free energy contributions of mixing and elasticity, respectively; χ, the Flory interaction parameter; N, the average degree of polymerization of the subchain between two neighbor crosslinking points; ϕ, the volume fraction of polymer; and ϕ_0, the initial volume fraction of polymer. The temperature dependence of χ can be expressed as [32]

$$\chi = \frac{\Delta F_m}{k_B T} = \frac{\Delta H_m - T\Delta S_m}{k_B T} \tag{4}$$

where ΔH_m and ΔS_m are the enthalpy and entropy changes of polymer–solvent mixing, respectively. The osmotic pressure Π is given by

$$\Pi = \phi^2 \frac{\partial(\Delta F/\phi)}{\partial\phi} \tag{5}$$

At swelling equilibrium, $\Pi = 0$. The phase diagram for a phantom network can be calculated from a combination of Eqs. (1)–(5) and

$$\frac{1}{T} = \frac{\Delta S}{\Delta H} + \frac{k_B}{\Delta H \phi_0^2}\left\{\frac{\phi_0}{N}(\alpha^3 - 2\alpha^5) - 2\alpha^6\ln\left(1 - \frac{\phi_0}{\alpha^3}\right) - 2\phi_0\alpha^3\right\} \tag{6}$$

where $\alpha = (\phi/\phi_0)$, a relative volume change.

Static Laser Light Scattering

For a dilute solution or colloidal dispersion at a small scattering angle the weight-average molecular or particle molar mass M_w can be related to the excess absolute time-averaged scattered light intensity (the Rayleigh ratio $[R_w(q)]$) by [33,34]:

$$\frac{KC}{R_{VV}(q)} = \frac{1}{M_c}\left(1 + \frac{1}{3}\langle R_g^2\rangle_z q^2\right) + 2A_2 C \tag{7}$$

where $K = 4\pi^2 n^2 (dn/dC)^2/(N_A\lambda_0^4)$ and $q = (4\pi n/\lambda_0)\sin(\Theta/2)$, with N_A, n, λ_0, and θ being Avogadro s number, the solvent refractive index, the wavelength of light in vacuo, and the scattering angle, respectively; C is the concentration (g/mL); $\langle R_g^2\rangle^{1/2}$ (written as $\langle R_g\rangle$) is the average radius of gyration; and A_2 is the second virial coefficient.

Dynamic Laser Light Scattering

A precise intensity–intensity time correlation function $G^2(t,q)$ in the self-beating mode was measured [33,34] and

$$G^{(2)}(t,q) = A[1 + \beta|g^{(1)}(t,q)|^2] \tag{8}$$

where A is a measured baseline; β, a parameter depending on the coherence of the detection; t, the delay time; and $g^{(1)}(t,q)$, the normalized electric field time correlation function which can be related to the linewidth distribution $G(\Gamma)$ by

$$g^{(1)}(t,q) = \int_0^\infty G(\Gamma)e^{-\Gamma t}d\Gamma \tag{9}$$

where the linewidth Γ is usually a function of both C and θ [35] $G(\Gamma)$ can be obtained from the Laplace inversion of $G^{(2)}(t,q)$. If the relaxation is diffusive, Γ/q^2 is equal to the translational diffusion coefficient D at $c \to 0$ and $q \to 0$. In this case, $G(\Gamma)$ can be converted to the translational diffusion coefficient distribution $G(D)$ or to the hydrodynamic radius distribution $f(R_h)$ by $R_h = k_B T/(6\pi\eta D)$, where k_B and η are the Boltzmann constant and solvent viscosity, respectively.

EXPERIMENTAL

Materials

N-Isopropylacrylamide (courtesy of Kohjin, Ltd., Japan) was recrystallized three times in a benzene/*n*-hexane mixture; *N,N'*-methylenebis(acrylamide) (BIS) as a crosslinker was recrystallized from methanol. Potassium persulfate (KPS) (from Aldrich, analytical grade), as an initiator, and sodium dodecyl sulfate (SDS) (from BDH, 99%), as a dispersant, were used without further purification.

Sample Preparation

The PNIPAM microgel particles were made by emulsion polymerization. 3.84 g PNIPAM, 0.0730 g BIS, and 0.0629 g SDS were added into 240 mL dust-free deionized water. A 500-mL reactor fitted with a glass stirring rod, a Teflon paddle, a reflux condenser, and a nitrogen bubbling tube was used. The solution was heated to 70°C and stirred at 200 rpm for 40 min with a nitrogen purge to remove oxygen. Finally, 0.1536 g KPS dissolved in 25 mL dust-free deionized water was added to start the reaction. The solution was stirred for another 4.5 h. The microgel particles were purified and diluted to $\sim 1 \times 10^{-5}$ to $\sim 1 \times 10^{-6}$ g/mL for further LLS measurements.

Laser Light Scattering

A commercial laser light scattering (LLS) spectrometer (ALV/SP-150) equipped with an ALV-5000 digital time correlator was used with a solid-state laser (ADLAS DPY425II, output power $\approx$400 mW at λ = 532 nm) as the light source. The incident light was vertically polarized with respect to the scattering plane, and the light intensity was regulated with a beam attenuator (Newport M-925B) to avoid a possible localized heating in the light-scattering cuvette. In our setup, the coherent factor β in dynamic LLS is $\sim$0.87. With some proper modifications [36], our LLS spectrometer is capable of recording both static and dynamic LLS continuously in the range of 6°–154°. The accessible small-angle range is particularly useful in the measurement of large microgel particles because the condition of $qR_g < 1$ is required to determine the precise values of M_w, R_g, and D.

RESULTS AND DISCUSSION

Figure 1 shows the angular dependence of the characteristic linewidth distributions $G(\Gamma/q^2)$ of the PNIPAM microgel particles, where $C = 1.18 \times 10^{-5}$ g/mL and $T = 15$°C. When $\theta \leq 20°$, only one peak with $\langle\Gamma\rangle/q^2 \sim 9.95 \times 10^{-9}$ cm^2/sec was observed. This peak is related to the translational diffusion of the microgel particles in water, from which we can calculate the hydrodynamic radius distribution $f(R_h)$. When $\theta \geq 90°$, a very small second peak (barely seen in Fig. 1) appears at $\langle\Gamma\rangle/q^2 \sim 1.45 \times 10^{-7}$ cm^2/sec. This small second peak reflects the internal motion of the PNIPAM subchains between two neighbor crosslinking points and it will be discussed in detail in a separate paper. The first peak is very narrow and nearly independent of θ in the range of $8° < \theta < 110°$. This angular independence indicates a spherical symmetry of the microgel particles. The average hydrodynamic radius $\langle R_h\rangle$ of the PNIPAM microgels is 190 ± 5 nm at $T = 15$°C.

Figure 2 shows the temperature (T) dependence of $\langle R_h\rangle$ in water. When $T <$ 31°C, the microgel particles shrink slightly as T increases. However, when T increases from 31°C to 35°C, the microgel particles undergo a dramatic, but continuous, volume change, which is in contrast with the discontinuous volume change observed in some bulk PNIPAM gels. The phase transition temperature of the microgel particles is ~33.0°C, similar to that of individual PNIPAM linear chains in water. Further increase of T had little effects on $\langle R_h\rangle$, which remained constant (~65 nm) when $T > 35$°C. After determining the temperature dependence of $\langle R_h\rangle$, we used static LLS to characterize the PNIPAM microgel particles at three different temperatures which correspond to the different stages of swelling and collapse.

Figure 3 shows a typical Zimm plot of the PNIPAM microgel particles in water, where $T = 35$°C, 2.95×10^{-6} g/mL $\leq c \leq 1.48 \times 10^{-5}$ g/mL; and $20° \leq \theta \leq 140°$. $KC/R_{vv}(q)$ depends linearly on both θ and C, M_w, $\langle R_g\rangle$, and A_2 was obtained from Eq. (7). As shown in Fig. 2, when $T \leq 30$°C, the microgel particles swelled in water and $\langle R_h\rangle$ is very large, so that an extrapolation of $KC/R_{vv}(q)$ in the small-angle range (6°–20°) is necessary. Table 1 summarizes the results of static

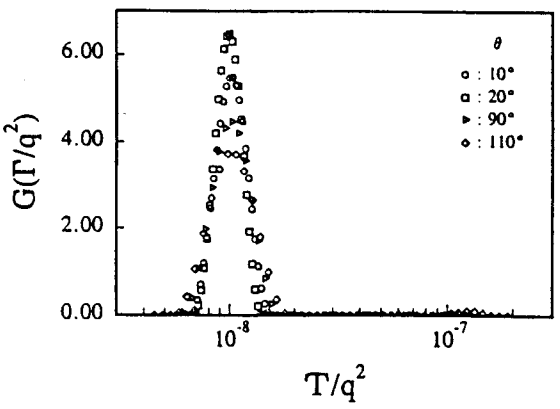

FIG. 1. Linewidth distributions $G(\Gamma/q^2)$ of the PNIPAM microgel particles in water at different scattering angles, where $T = 15$°C and $C = 1.182 \times 10^{-5}$ g/mL.

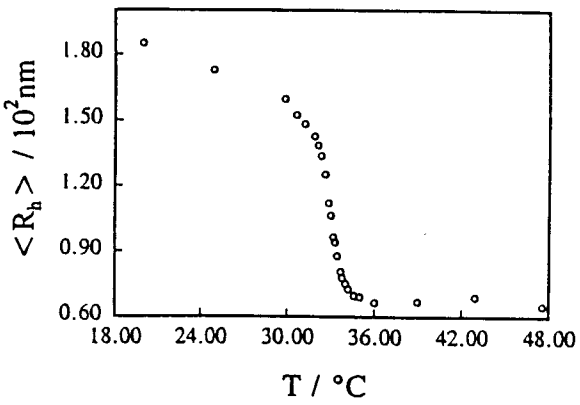

FIG. 2. Average hydrodynamic radius $\langle R_h \rangle$ of the PNIPAM microgel particles as a function of the solution temperature.

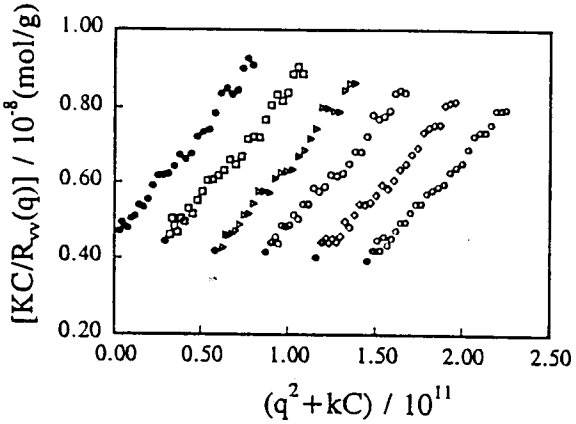

FIG. 3. Typical Zimm plot of the PNIPAM microgel particles in water, where T = 35°C and C ranges from 2.95×10^{-6} to 1.48×10^{-5} g/mL.

TABLE 1

Laser Light Scattering Results for the PNIPAM Microgel Particles in Water at Two T Values

	Microgel particles							Linear chain		
T (°C)	dn/dC (mL·g^{-1})	M_w (g/mol)	A_2 (mol·ml/g^2)	R_g (nm)	R_h (nm)	R_g/R_h	ρ (g·mL^{-1})	R_g/R_h	ρ (g·mL^{-1})	dn/dC (ml·g^{-1})
30.01	0.181	2.19×10^8	3.02×10^{-6}	124	160	0.78	0.021	1.52	0.0063	0.167
35.01	0.201	2.25×10^8	-2.25×10^{-5}	57	70	0.81	0.30[a]	0.65[a]	0.20[a]	0.171[a]

[a]Represent the values at the collapsing limit.

LLS measurements at $T = 30°C$ and $T = 35°C$. The large dn/dC increase from 0.181 mL · g^{-1} at T = 30°C to 0.201 mL · g^{-1} at T = 35°C is attributed to the increase in the PNIPAM chain segment density ρ from 0.021 g/cm^3 to 0.30 g/cm^3, where ρ was calculated by $\rho \sim M_w/[N_A(4/3)\pi R_h^3]$. On the basis of the ρ and R_h values in Table 1, we know that ~94% of water inside the swollen microgel network is driven out during the phase transition. The independence of M_w from temperature indicates that there is no aggregation, which would be expected to increase with T. Both $\langle R_g \rangle$ and A_2 decrease as T increases from 30°C to 35°C. The decrease of $\langle R_g \rangle$ reflects the clear collapse of the microgel particles. The change of A_2 from positive to negative indicates that water becomes a poor solvent at 35°C, just as for individual PNIPAM chains in water. The Θ temperature (~31°C) of the PNIPAM microgel in water, as estimated from the temperature dependence of A_2, was similar to that of individual chains.

In Table 1 we compare results of the microgels with those of linear PNIPAM chains, whose M_w and M_w/M_n are 1.08×10^7 g/mol and 1.05, respectively. For PNIPAM microgel particles in water, $\langle R_g \rangle/\langle R_h \rangle$ (~0.78 ± 0.03) is very close to 0.774, predicted for a uniform hard sphere [37]. The temperature independence of $\langle R_g \rangle/\langle R_h \rangle$ shows that even in the swollen state the microgel particles are homogeneous in density, because in the microgel network the subchains are short and uniformly distributed. The value of $\langle R_f \rangle/\langle R_h \rangle \sim 0.78$ also shows that the microgel particles are nondraining; that is, all water molecules in the interior move with the microgel network. This constant $\langle R_g \rangle/\langle R_h \rangle$ value suggests that the collapse speed in the center of the particle is the same as near the surface. This contrasts with the behavior of individual PNIPAM linear chains in water, where $\langle R_g \rangle/\langle R_h \rangle$ decreases dramatically from ~1.52 to ~0.65 in the same temperature range, and the chain conformation changes from an extended coil to a collapsed globule. This difference between the PNIPAM microgel particles and individual PNIPAM linear chains is understandable. When $T \leq 30°C$, water is a good solvent and the PNIPAM linear chain with an extended coil conformation is draining, which leads to a smaller R_h and a higher $\langle R_g \rangle/\langle R_h \rangle$ value (~1.5). During the collapse, some water, especially that in the center of the coil, is expelled, so that the coil become less draining so that $\langle R_h \rangle$ approaches the outside radius of the collapsed coil. The portion of the chain in the center of the coil should be less solvated and more compacted. Therefore, the density in the center of the collapsed single-chain globule is higher than that near the surface. This is why $\langle R_f \rangle/\langle R_h \rangle$ is even lower than the value of 0.774 predicted for a uniform sphere. Table 1 shows that the chain density ρ of the PNIPAM microgel network is only ~30 g/cm^3 even in the collapsing limit, which is in agreement with that of bulk gels studied by small-angle neutron scattering [21]. This low chain density was explained by Grosberg and Nechaev in terms of the concept of the crumpled globule state [16]. In comparison with the chain density ($\rho \sim 0.20$ g/cm^3) of the PNIPAM linear chain in the globule state, the chain density of the microgel at its collapsing limit is slightly higher, but still much lower than the density (~1 g/cm^3) of bulk PNIPAM. In contrast, the chain density of the swollen microgel particles in the swollen state is ~4 times higher than that of the PNIPAM linear chains under the same conditions. This difference in the swelling capability can be better demonstrated by the expansion factor α.

Figure 4 shows the expansion factor $\alpha_h[\equiv \langle R_h \rangle/\langle R_h \rangle^*]$ as a function of temperature, where $\langle R_h \rangle^*$ is the hydrodynamic radius at the collapsing limit. The

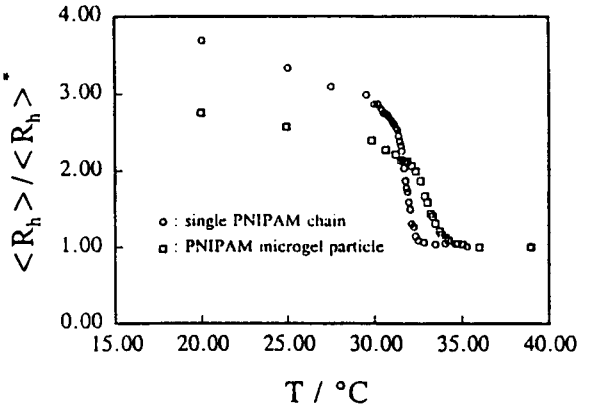

FIG. 4. Expansion factor α_h [$\equiv \langle R_h \rangle / \langle R_h \rangle^*$] as a function of temperature for the PNIPAM microgel particles and individual chains ($M_w = 1.08 \times 10^7$ g/mol and $M_z/M_w \sim 1.05$), where $\langle R_h \rangle^*$ is the average hydrodynamic radius at the collapsing limit.

open circles (○) represent the PNIPAM linear chains ($M_w = 1.08 \times 10^7$ g/mol and $M_Z/M_W < 1.05$) in water at $C = 4.60 \times 10^{-6}$ g/mL; and the open squares represent (□) the microgel particles in water at $C = 1.18 \times 10^{-5}$ g/mL. Both of the volume changes are continuous. Three features in Fig. 4 should be noted. First, as expected, the linear chains swell much more than the microgel particles in the good solvent region. Second, the phase transition of the microgel particles is less sharp. In the past, this less-sharp phase transition was attributed to the irregularity of particle surface and the inhomogeneous particle size. This would make the phase transition of individual PNIPAM linear chains even less sharp because a linear chain has a wide distribution of chain extensions. We believe that the less-sharp phase transition of the microgel particles is due to different lengths of the subchains in the microgel network. It is known that for a given polymer concentration, polymer chains with different lengths undergo a phase transition at different temperatures. Third, the phase transition temperature of the microgel particles is -1.5°C higher than that of the PNIPAM linear chains. The difference can also be explained in terms of the difference in the chain length. In comparison with the high molecular weight PNIPAM linear chain, the subchain between two neighbor crosslinking points inside the microgel network is much shorter. Qualitatively, the higher phase transition temperature can also be explained on the basis of Eqs. (1) and (3). For the linear chains, $\Delta F = \Delta F_m$, while for the microgel particles, $\Delta F = \Delta F_m + \Delta F_{el}$. In a good solvent, $\Delta F < 0$, and both the linear chains and the microgel particles are swollen. When $\Delta F > 0$, the segment–segment interaction is stronger than the solvent–segment interaction so that the linear chains and the microgel particles collapse [40]. According to Eq. (3), when a gel is swollen, $\alpha > 1$ and $\Delta F_{el} > 0$. The elasticity will retard the chain expansion in a good solvent. When a gel is shrunken, $\alpha < 1$ and $\Delta F_{el} < 0$. ΔF_{el} contributes negatively to ΔF and the elasticity prevents the gel collapse in a poor solvent. Therefore, the collapse of a linear chain is easier than that of a gel. Equation (3) also shows that ΔF_{el} is inversely proportional to N. This implies that in a poor solvent, the higher the crosslinking density (the smaller N), the higher the transition temperature, as experimentally confirmed [38].

Figure 5 shows the scattered light intensity $\langle I \rangle$ of the microgel particles as a function of temperature, where $\theta = 20°$ and $C = 1.182 \times 10^{-5}$ g/mL. The increase of $\langle I \rangle$ at $T > \Theta$ is attributed to the increase of dn/dC that is:

$$\left(\frac{dn}{dC}\right)^2_{T=35°C} \approx 1.2\left(\frac{dn}{dC}\right)^2_{T=30°C}$$

In contrast, the dn/dC of the linear PNIPAM chain in water is independent of temperature even at $T > \Theta$. This difference in the temperature dependence of dn/dC implies that individual PNIPAM linear chains and the microgel particles might reach different collapsed states.

Our results (not shown) indicate that the distribution of the hydrodynamic radius is time independent show that the collapsed microgel particles in water are thermodynamically stable. No aggregation was detected even for 1 week at $T =$ 39°C. By contrast, the single PNIPAM linear chains are only kinetically stable in the collapsing limit ($T \geq 33$°C) and the interchain aggregation occurs after $\sim 10^3$ sec even in very dilute solution [39].

Figure 6 shows the collapsing and swelling kinetics (in terms of $\langle R_h \rangle$) of the microgel particles, where t is the standing time after the solution was quenched from 35.0°C to 30.0°C, or inversely jumped from 30°C to 35°C. In order to speed up the temperature equilibrium, a very special thin-wall (~ 0.4 mm) LLS cuvette was used. Both the swelling and collapse are too fast to follow by our procedure. As stated before, for a spherical gel, $t = R^2/\pi^2 D$. Here, the radius of the microgel particles at $T = \Theta$ is ~ 150 nm and the collective diffusion coefficient D_c is $\sim 10^{-7}$ cm^2/sec, so that $t \sim 10^{-4}$ sec. In comparison, the coil-to-globule transition of the high molecular weight linear PNIPAM chain is much slower. This difference in the transition speed is due to the fact that the subchain between two crosslinking points in the microgel particles is $\sim 10^2$ times shorter than the length of the high molecular weight linear PNIPAM chains [41]. Moreover, the swelling or shrinking speed of a gel in response to an excess osmotic pressure is controlled by the collective diffusion

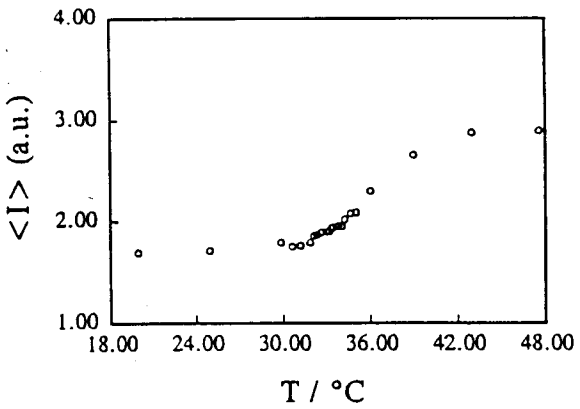

FIG. 5. Scattered light intensity $\langle I \rangle$ of the PNIPAM microgel particles in water as a function of the solution temperature, where $C = 1.182 \times 10^{-5}$ g/mL, $\theta = 20°$, and the units are arbitrary.

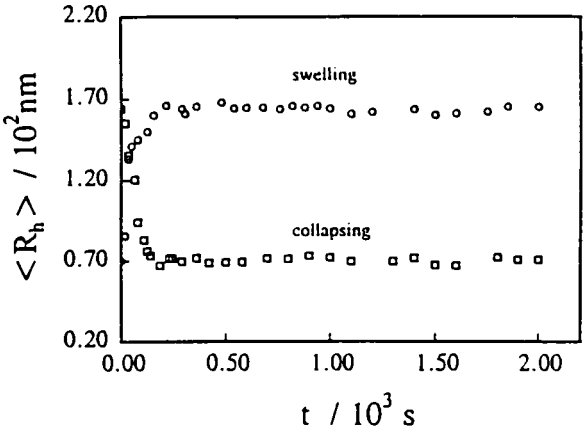

FIG. 6. Collapsing and swelling kinetics of the PNIPAM microgel particles, after the solution temperature abruptly changes from 30.0°C to 35.0°C, or inversely.

of solvent into the gel. The very large surface-to-volume ratio of the microgel particles leads to a very fast swelling or shrinking in comparison with bulk gels. In addition, the coil-to-globule transition of the longer linear PNIPAM chain in water involves the intrachain penetration (knotting) and rearrangement of the collapsed chain, which requires a relatively long time [39].

ACKNOWLEDGMENTS

The financial support of the RGC (Research Grants Council of Hong Kong) Earmarked Grant 1994/95 (CUHK 453/95P, 221600460) is gratefully acknowledged.

REFERENCES

1. K. Dusek and D. Patterson, *J. Polym. Sci., Phys. Ed.* 6, 1209 (1968).
2. J. Hasa, M. Ilavsky, and K. Dusek, *J. Polym. Sci., Polym. Phys. Ed.* 13, 253 (1975).
3. T. Tanaka, *ACS Symp. Ser., 480*, 1 (1991), and references therein.
4. M. Shibayama and T. Tanaka, *Adv. Polym. Sci., 109*, 1 (1991), and references therein.
5. Y. Osada and S.B. Ross-Murphy, *Sci. Am., 264*, 42 (1993).
6. M. Ilavsky, *Macromolecules, 15*, 782 (1982).
7. T. Tanaka, D. Fillmore, S. T. Sun, I. Nishio, G. Suislow, and A. Shah, *Phys. Rev. Lett., 45*, 1636 (1980).
8. T. Tanaka, I. Nishio, S. T. Sun, and S. U. Nishio, *Science, 218*, 467 (1982).
9. A. Suzuki and T. Tanaka, Nature, 346, 345 (1990).
10. B. Erman and P. J. Flory, *Macromolecules, 19*, 2342 (1986).
11. U. Hirokawa, T. Tanaka, and E. S. Matsuo, *J. Chem. Phys, 81*, 6379 (1984).
12. R. F. S. Freitas and E. L. Cussler, *Sep. Sci. Technol, 22*, 911 (1987).
13. S. Hirotsu, Y. Hirokawa, and T. Tanaka, *J. Chem. Phys., 87*, 1392 (1987).
14. S. Hirotsu, *Adv. Polym. Sci., 110*, 1 (1993).
15. K. Otake, H. Inomata, M. Konno, and S. Saito, *J. Chem. Phys., 91*, 1345 (1980).
16. M. Marchetti, S. Prager, and E. L. Cussler, *Macromolecules, 23*, 1760 (1990).

17. A. Grosberg and S. K. Nechaev, *Macromolecules, 24*, 2789 (1991).
18. K. Otake, H. Inomata, M. Konno, and S. Saito, *Macromolecules, 23*, 283 (1990).
19. Y. Hirokawa, E. Sato, S. Hirotsu, and T. Tanaka, *Polym. Mater. Sci. Eng., 52*, 520 (1985).
20. Y. Li. and T. Tanaka, J. Chem. Phys., 90, 5161 (1989).
21. M. Tokita and T. Tanaka, *Science, 253*, 1121 (1991).
22. M. Shibayama and T. Tanaka, *J. Chem. Phys., 97*, 6829 (1992).
23. M. V. Badiger, P. R. Rajamohanan, M. G. Kulkarni, S. Ganapathy, and R. V. Mashelkar, *Macromolecules, 24*, 106 (1991).
24. T. Tanaka, E. Sato, Y. Hirokawa, S. Hirotsu, and J. Peetermans, *Phys. Rev. Lett., 55*, 2455 (1985).
25. E. Sato and T. Tanaka, *J. Chem. Phys., 89*, 1695 (1988).
26. Y. Hirose, T. Amiya, Y. Hirokawa, and T. Tanaka, *Macromolecules, 20*, 1342 (1987).
27. M. J. Snowden, B. Vincent, and J. C. Morgan, U. K. Patent GB2262117A (1993).
28. R. H. Pelton and P. Chibante, *Colloids Surf., 20*, 247 (1986).
29. W. McPhee, K. C. Tam, and R. H. Pelton, *J. Colloid Interface Sci., 156*, 24 (1993).
30. M. Murray, F. Rana, I. Haq, J. Cook, B. Z. Chowdhry, and M. J. Snowden, *J. Chem. Soc., Chem. Commun., 18*, 1803 (1994).
31. B. E. Rodriguez and M. S. Wolfe, *Macromolecules, 27*, 6642 (1994).
32. M. Moerkerke, *Macromolecules, 28*, 1103 (1995).
33. B. H. Zimm, *J. Chem. Phys., 16*, 1099 (1948).
34. P. Debye, *J. Phys. Coll. Chem., 51*, 18 (1947).
35. R. Pecora, *Dynamic Light Scattering*, Plenum Press, New York, 1976.
36. B. Chu, Laser Light Scattering (2nd Ed.), Academic Press, New York, 1991.
37. W. H. Stockmayer and M. Schmidt, *Pure Appl. Chem., 54*, 407 (1982); *Macromolecules, 17*, 509 (1984).
38. C. Wu, K. Chan, and K. Q. Xia, *Macromolecules, 28*, 1032 (1995).
39. M. Schmidt, D. Nerger, and W. Burchard, *Polymer, 20*, 581 (1979).
40. M. Shibayama, M. Morimoto, and S. Nomura, *Macromolecules, 27*, 5060 (1994).
41. C. Wu and S. Q. Zhou, submitted for publication.

Received April 23, 1996
Revised July 16, 1996
Accepted July 19, 1996